

Supplementary Information for: Macromolecular Crowding Induces Spatial Correlations that Control Gene Expression Bursting Patterns

S. Elizabeth Norred^{1,2}, Patrick M. Caveney^{1,2}, Gaurav Chauhan³, Lauren K. Collier¹, C. Patrick Collier¹, Steven M. Abel³, Michael L. Simpson^{*,1,2}

¹Center for Nanophase Materials Sciences, Oak Ridge National Laboratory, Oak Ridge, TN, 37831

²Bredesen Center for Interdisciplinary Research and Graduate Education, University of Tennessee Knoxville/Oak Ridge National Laboratory

³Chemical and Biomolecular Engineering Department, University of Tennessee Knoxville, Knoxville, TN, 37996

*Corresponding author: SimpsonML1@ornl.gov

Table of Contents

Expression Burst Analysis	3
Model Description and Supplemental Figures	7
Figure S1	7
Figure S2	8
Figure S3	9
Physical Model of Expression in Crowded Environments	10
Figure S4	13
Table S1	14
Figure S5	15
Figure S6	16
Figure S7	17
Experimental Methods Supplement	18
Gene Structure and Preparation	18
Cell-Free Experimental Methods	18
Vesicle Preparation Methods	19

Expression Burst Analysis

Gene expression noise may be characterized using various measures based on the mean value (μ) of a reporter (e.g. fluorescent protein) of a molecular population (e.g. number of mRNA or protein molecules) and the variance (σ^2) of the distribution of these molecular populations. Common measures include coefficient of variation (CV), the square of the coefficient of variation (CV^2), and the Fano factor (FF). These three measures of the relative magnitude of expression variations are related as follows:

$$CV^2 = \frac{\sigma^2}{\mu^2}$$
$$CV = \sqrt{CV^2}$$
$$FF = \frac{\sigma^2}{\mu} = \mu CV^2$$

The Fano factor, which has also been known as noise strength¹ or just defined mathematically² as μCV^2 , has been used at least since 2001¹ as a direct measure of burst size. Ozbudak et al. experimentally demonstrated³ that the Fano factor was linearly related to the translational burst size (the average number of proteins produced from an individual mRNA template), and Hasty and Collins⁴ commented that these results showed some evidence of transcriptional bursting. So et al. used Fano factor measurements to demonstrate that in *E. coli*, an increased transcriptional rate is often accomplished by an increased transcriptional burst size⁵. Taniguchi et al. showed in *E. coli* that the Fano factor of the protein noise increased approximately linearly with increasing protein population⁶, and later analysis showed that this relationship was due to burst size increasing linearly with the protein population⁷. Other studies have used the Fano factor to characterize the transcriptional burst size in expression controlled by the HIV LTR promoter^{2, 8, 9}.

Some studies that did not explicitly use the Fano factor as a measure of expression burst size, still used the same underlying Fano factor principle to interpret their results. For example, Hansen et al. noted¹⁰ that in their cell-free expression experiments that increased macromolecular crowding led to a larger CV^2 without a correspondingly large

decrease in their measured μ . However, since $FF = \mu CV^2$, their experimental results demonstrated a crowding induced increase in the Fano factor in a way entirely consistent with the results reported here.

Although the three commonly used measures of noise are closely related, the Fano factor is the measure that is most strongly associated with burst size (B). Conversely, since

$$CV^2 = \frac{FF}{\mu} \propto \frac{B}{\mu}$$

and

$$\mu \propto B f_B,$$

then⁷

$$f_B \propto \frac{1}{CV^2},$$

where f_B is the burst frequency. Accordingly, throughout this work we use the Fano factor as a measure of burst size and $1/CV^2$ as a measure of burst frequency.

Looking deeper at the relationship between burst size and Fano factor, we can approximate expression bursting as the product of two random processes: Process A (transcriptional initiation) composed of a Poissonian pulse train of impulse functions of weight = 1 and average value \bar{A} ; and Process B (expression bursting) that is uncorrelated with process A, has a mean value of \bar{B} , and a variance of σ_B^2 (note: we have lumped transcriptional and translational bursting into a single process with an average burst size of \bar{B})

$$\phi_A(\tau) = \bar{A}\delta(\tau) + \bar{A}^2$$

$$\phi_B(\tau) = \sigma_B^2\delta(\tau) + \bar{B}^2$$

The autocorrelation function of the expression burst is given by the product of the autocorrelation functions of these two functions, or

$$\phi_{AB}(\tau) = \phi_A(\tau) * \phi_B(\tau) = \bar{A}\sigma_B^2\delta(\tau) + \bar{A}\bar{B}^2\delta(\tau)$$

where we have neglected all the \bar{A}^2 terms because $\bar{A} \ll 1$. From this we get

$$\sigma_{AB}^2 = \bar{A}\bar{B}^2 + \bar{A}\sigma_B^2$$

and the Fano factor (which would be the Fano factor of the protein abundance) is

$$FF_{AB} = FF_{\langle P \rangle} = \frac{\sigma_{AB}^2}{\bar{A}\bar{B}} = \bar{B} + \frac{\sigma_B^2}{\bar{B}}$$

or

$$FF_{\langle P \rangle} = (\bar{B} + FF_B),$$

where FF_B is the Fano factor of the expression burst size.

Most previous analyses have assumed that expression bursting represents the counting of a Poissonian pulse train^{1, 11}, in which case

$$FF_{\langle P \rangle} = (\bar{B} + 1)$$

is the result. Yet, this often-used equation becomes inaccurate when there is greater variability in the expression burst size. As an example, consider a case where the expression burst size distribution is split between a high (B_H) and a low (B_L) level. This would be a simple approximation for an inhomogeneous spatial distribution of resources where some regions are prone to very high translation rates, while other regions produce protein at relatively low rates. In this case

$$\bar{B} = P_H B_H + (1 - P_H) B_L \approx P_H B_H$$

$$\sigma_B^2 \approx P_H (1 - P_H) B_H^2$$

$$FF_B \approx \frac{P_H (1 - P_H) B_H^2}{P_H B_H} = (1 - P_H) B_H$$

$$FF_p \approx \bar{B} + (1 - P_H) B_H = P_H B_H + (1 - P_H) B_H = B_H$$

where P_H is the probability of having the B_H -sized translational burst. The approximation in these equations assumes that $P_H B_H \gg B_L$. Since $F_{Bapp} \propto \frac{1}{CV^2}$, where F_{Bapp} is the apparent burst frequency,

$$F_{Bapp} \propto \frac{\langle P \rangle}{FF_p} \propto \frac{P_H B_H F_B}{B_H} = P_H F_B$$

where F_B is the actual burst frequency. So, for the bursting case analyzed above, the apparent burst size is B_H not \bar{B} , and the apparent burst frequency is $P_H F_B$ not F_B . In other words, as long as $P_H B_H \gg B_L$, the train of high bursts completely control the noise behavior.

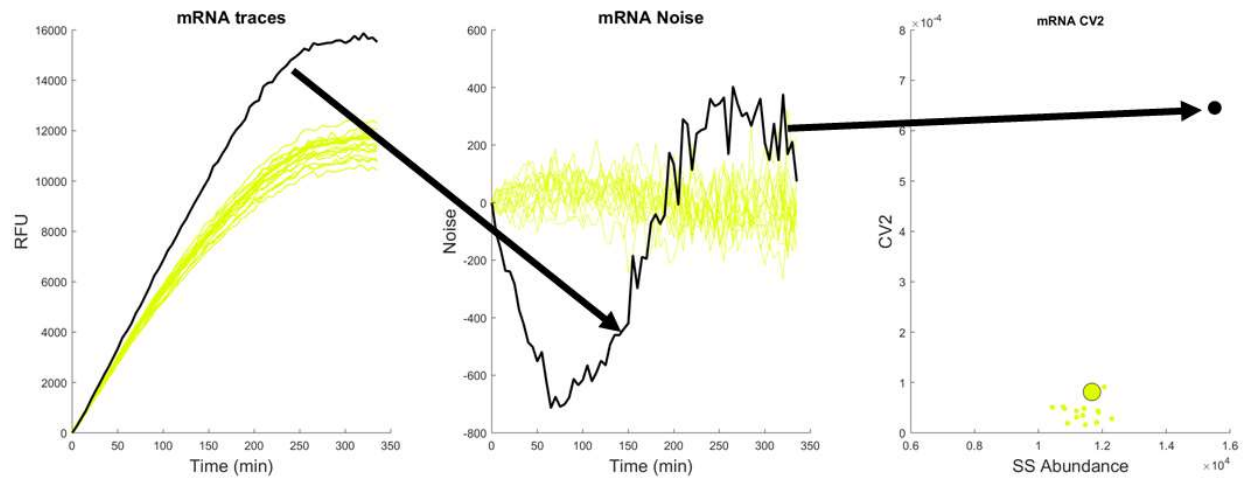


Figure S1: “Outlier” behavior in transcription in 5% crowding fraction experiment. A) The individual outlier expression trace is shown here in black. The yellow lines indicate expression traces found in the same experiment. B) Individual noise traces are shown as colored lines. Outlier noise trace shown in black. These outliers typically have high CV^2 values. C) Individual noise values shown as small dots. Mean CV^2 for this experiment shown as a large dot. Outlier noise value shown as black dot.

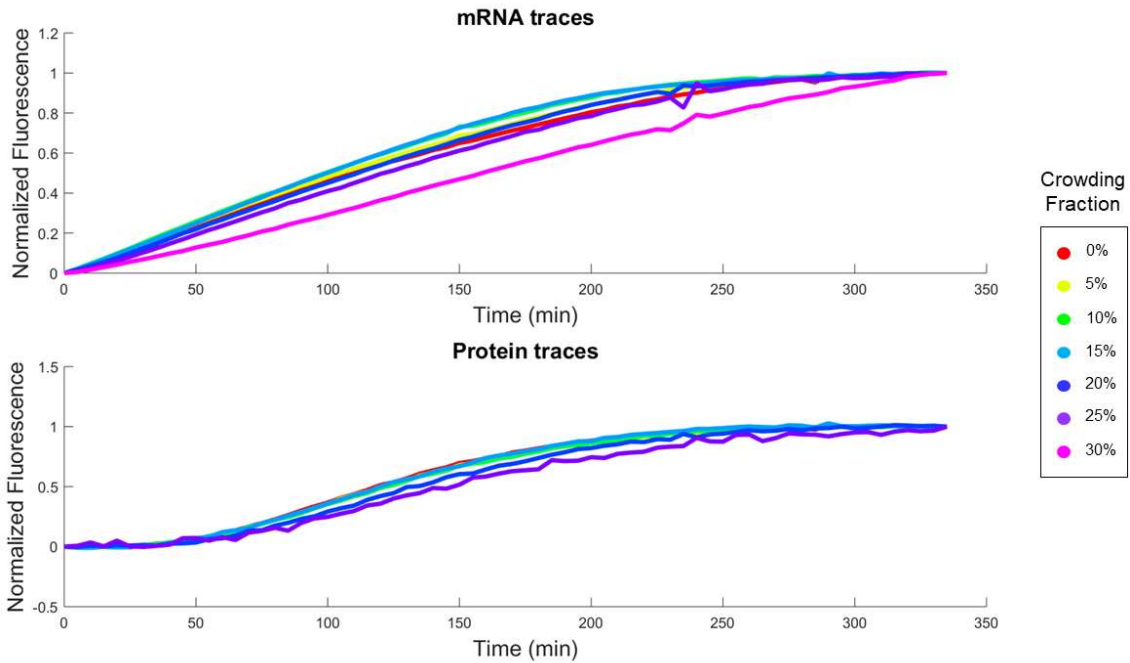


Figure S2: Normalized traces of average protein and mRNA expression. Normalized general trends across all crowding fractions up to 25% demonstrate similar shape and behavior over time. Notably, the 30% crowding fraction trace for mRNA appears to deviate from the other trends. No protein expression was detected at the 30% crowding fraction.

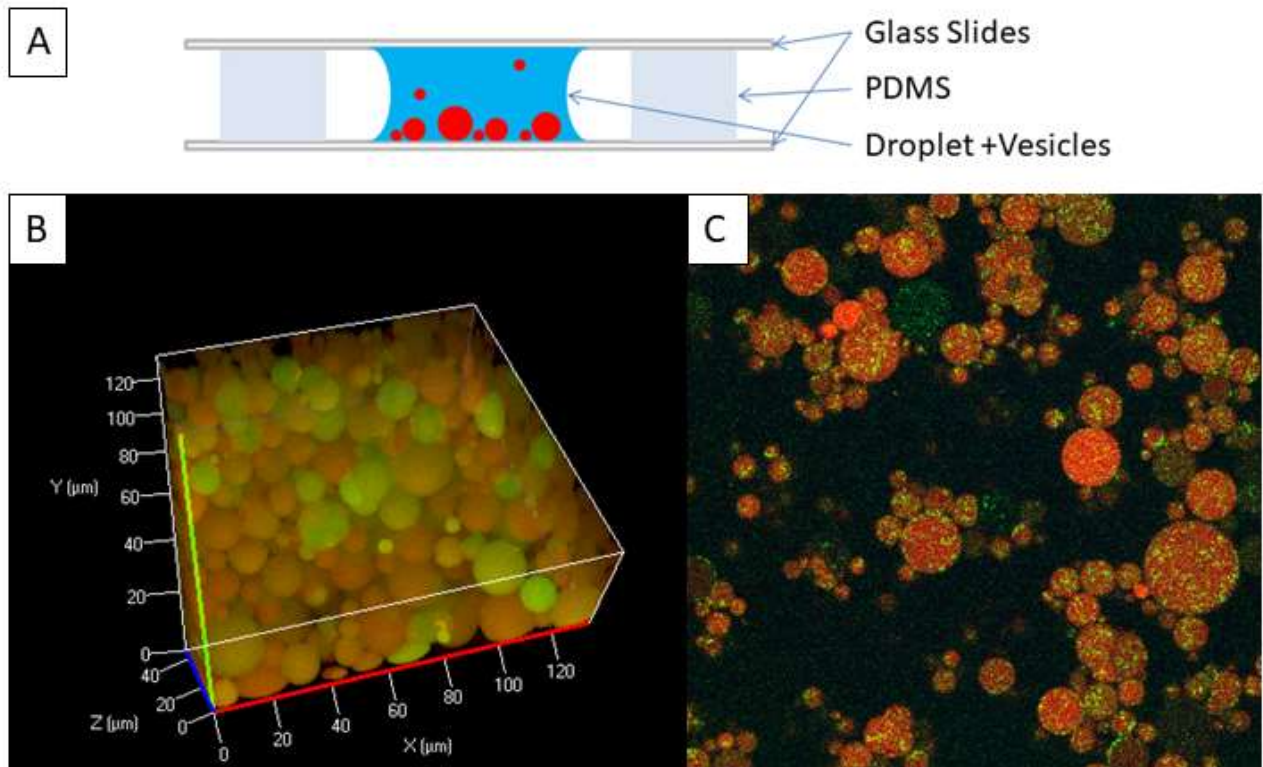


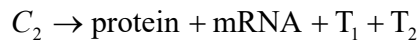
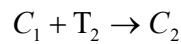
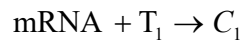
Figure S3: Protein synthesis in polydisperse vesicle microreactors. A) An ~10uL droplet containing the vesicles is placed on a glass coverslip, and surrounded by a PDMS spacer. The PDMS spacer is attached to the glass by plasma cleaning both layers, fixing the PDMS to the glass, and heating the layers at 80°C. These steps prevent delamination of the PDMS layer once the droplet is applied. Once the droplet has been added to the lower coverslip, another coverslip is placed on top of the PDMS spacer. This assembly allows the vesicles to be viewed over many hours at the interface of the glass, without risk of evaporation. B) Example of reconstructed 3D image of polydisperse vesicles sitting on the glass interface. These vesicles are expressing Green Fluorescent Protein and contain a red fluorescent volume marker. C) Example of 2D image slice of 5% crowded vesicles expressing pRSET-b-mCherry-Spinach2 in presence of DFHBI-1T.

Physical Model of Expression in Crowded Environments

We developed a physically motivated model in which (i) transcription and translation occur in compartmentalized regions of space, (ii) multiple components must assemble for translation to occur, and (iii) crowding influences the size of the compartmentalized regions and the transport of molecules to and from the regions. Increased crowding leads to slower diffusion and, at sufficiently high levels, likely leads to the emergence of isolated regions of transcription and translation that decrease in size as crowding increases.

Consider a system that contains N_c distinct locations at which mRNA is transcribed. Each of these locations is associated with a physical region of space (a “compartment”) in which transcription and translation occur. Each compartment has volume V_c and is regarded as well-mixed and independent of the others. As crowding increases, the crowding molecules decrease the volume of each compartment. The total volume of the system is conserved so that $V_{\text{tot}} = V_{\text{nc}} + N_c V_c$, where V_{nc} is the volume outside of the compartments. No reactions occur in this region, but reactants can diffuse from one compartment to another through it. Since the volume of the region outside of the reaction compartments increases with increasing crowding, we use V_{nc} as a proxy to describe the extent of crowding.

Within each compartment, mRNA is produced at rate α and translation is modeled as a series of two bimolecular reactions involving translational components T_1 and T_2 :



The sequence of reactions is motivated by the cooperative binding of multiple chemical species that is needed for translation to occur. We formulate the kinetics in terms of discrete numbers of molecules, so that the binding rates are given by $k_{\text{on},i} = k_{\text{on},i}^{(0)}/V_c$ for

$i=1,2$. Here, $k_{\text{on},i}^{(0)}$ is the second-order rate constant that would appear in a well-mixed system with kinetics formulated in terms of concentrations. The expression for $k_{\text{on},i}$ emphasizes that decreasing V_c leads to higher effective second-order rates within compartments. Hence, small compartment volumes promote binding of mRNA and translational components, as well as rapid rebinding after protein production. The rate of transcription (α) and the rate of protein production (k_p) decay exponentially in time to account for the decay in synthesis observed in cell-free reactions with time constants τ_α and τ_{k_p} respectively. Initially, the translational components are populated at random so that the probability of being in a particular region is equal to its fraction of the total volume. Each translational component can transition from the non-compartmental region to a compartment and vice versa. The entry rate into a compartment is Γ and the exit rate is γ . These values are constrained such that the net flux of translational components across compartmental boundaries is zero in the absence of mRNA: $\Gamma/\gamma = V_c/V_{\text{nc}}$. Since crowding impedes diffusion, the rates of entry and exit decrease with increasing V_{nc} . Bulk diffusion rates for a wide variety of molecular species decrease by about a factor of 30 over the range of crowding that we investigated experimentally¹². To match this magnitude of change in diffusion rates, we assumed the linear relationships $\Gamma = (1 - V_{\text{nc}})\Gamma_0$ and $\gamma = (1 - V_{\text{nc}})\gamma_0$ and allowed V_{nc} to vary between 0.1 and 0.97. Due to their larger size, we assume that the complexes C_1 and C_2 remained confined within a compartment once formed.

To analyze the model, we generated stochastic simulation trajectories using the Gillespie algorithm and tracked the number of mRNA and proteins over time. Noise analysis on the resulting trajectories was performed using the same procedure as for experimental results.

Main text Fig. 4D shows representative simulation trajectories for two values of V_{nc} that represent low ($V_{\text{nc}} = 0.10$) and high ($V_{\text{nc}} = 0.97$) levels of crowding. Trajectories

associated with the higher crowding level are more highly variable and, by inspection, appear to have episodic periods of rapid protein production. Main text Fig. 4E displays results of the noise analysis for simulations ranging from low to high crowding levels. The number of proteins decreases with increasing crowding, with a corresponding increase in CV^2 at large values of V_{nc} . The Fano factor increases markedly in this regime as well.

Physically, as the crowding increases, fewer translational components are found in reaction compartments. Additionally, their mobility decreases, leading to a slower sampling of the entire system volume. As a consequence, the waiting time to assemble a full translational complex (C_2) increases and the average number of proteins decreases. This is associated with a decrease in burst frequency. However, once all of the translational components are colocalized within a compartment, they are likely to rapidly rebind when the compartment volume is small. This has the effect of increasing burst size at large values of V_{nc} , which is reflected by the results in main text Fig. 4F.

To study explicitly the effect of translational burst size variability on protein noise, we constructed a simplified two-state expression model (Fig. S4) that captured the variability of the translational burst size predicted by the model described above. In this model, the average translational burst size remained constant, but the variance of the burst size increased with increasing crowding. In agreement with the measurements, the burst frequency ($\sim k_{on}$ in the model) was reduced as the crowding increased. Although the distribution of the translational burst size was not measured explicitly, the spatial organization of the mRNA population suggested a distribution with a high degree of skew and kurtosis (main text Fig. 4B). Accordingly, we chose a simple bimodal distribution with one high and one low translational burst size, where increased crowding led to greater separation between the low and high states without affecting the average translational burst size (Fig. S4B). Gillespie simulations of this model were performed where the variance of the burst size varied between 1x and 25x the mean burst size, and demonstrate that large variability in the translational burst size – not just

changes in the mean burst size – can generate the crowding-induced changes in protein noise behavior measured here (Fig. S4D).

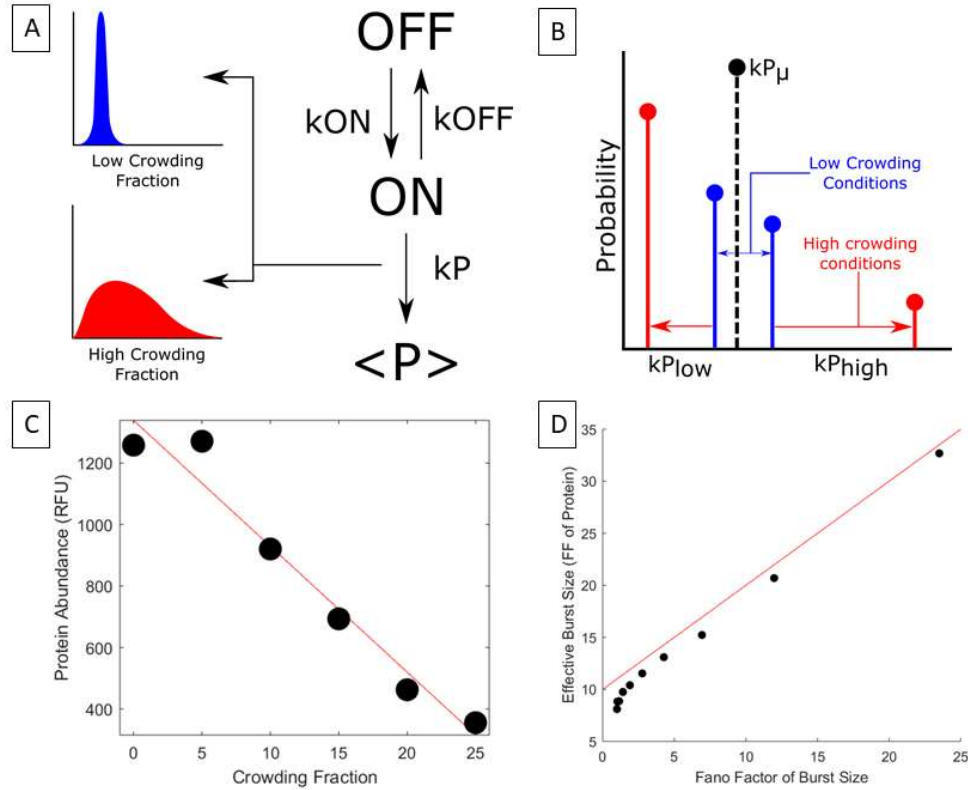


Figure S4: Simplified two-state expression model. A) A simplified two-state model of expression which allows modelling of a crowding-controlled distribution of translational burst sizes. B) Simple bimodal distribution of translation rate constant (k_p in (A)) used in the simulations. At low crowding levels k_{phigh} and k_{plow} were nearly equal. At higher crowding levels k_{phigh} and k_{plow} were further apart and the probability of k_{phigh} was reduced. (C) The variation of k_{ON} with crowding fraction for the simulations was found from a linear fit ($y = -40.96x + 1339$; red line) to the protein abundance vs crowding fraction measurements. (D) Gillespie simulation of the two-state model in (A) showing the relationship between the measured burst size (Fano factor of the protein) and Fano factor of the burst size. These simulations used the translation rate distributions in (B) and assumed an average burst size of 10. The red line uses the relationship in main text Eq. (1) with $\bar{B} = 10$.

Table S1: List of Model parameters used

N_c	10
Total number, T1	10
Total number, T2	10
α	0.01 s^{-1}
$k_{on,1}^{(0)}$	0.0001 s^{-1}
$k_{on,2}^{(0)}$	0.03 s^{-1}
k_p	20.0 s^{-1}
γ^0	0.7 s^{-1}
I^0	$\gamma^0 V_c/V_{nc}$
τ_α	55.55 min
τ_{kp}	27.78 min

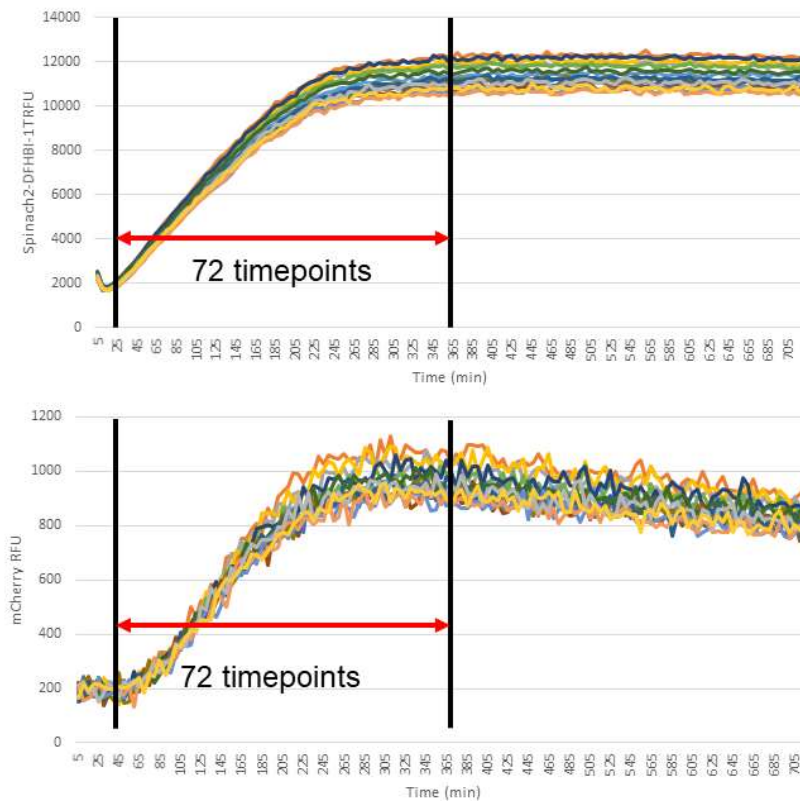


Figure S5: Protein and mRNA expression in PURExpress protein synthesis kit. A timescale of Spinach2-DFHBI-1T and mCherry fluorescence was read at 5 minute timesteps over 720 minutes. Each of the 16 time traces represents a single 15 μ L reaction; each individual color in both graphs corresponds to mRNA or protein expression from one reaction. All time traces used in this work were truncated at 72 time points (denoted by the red arrows), after all traces in all experiments reached maximum expression in both mRNA and protein. Steady state fluorescence shown afterward does not correspond to equilibrium between expression and decay, but rather is governed by the elimination of resources and buildup of toxic side-reactions and by-products^{13, 14}. The first 5 time points were excluded as the Spinach2-DFHBI-1T readings likely correspond to initial autofluorescence, and not mRNA expression.

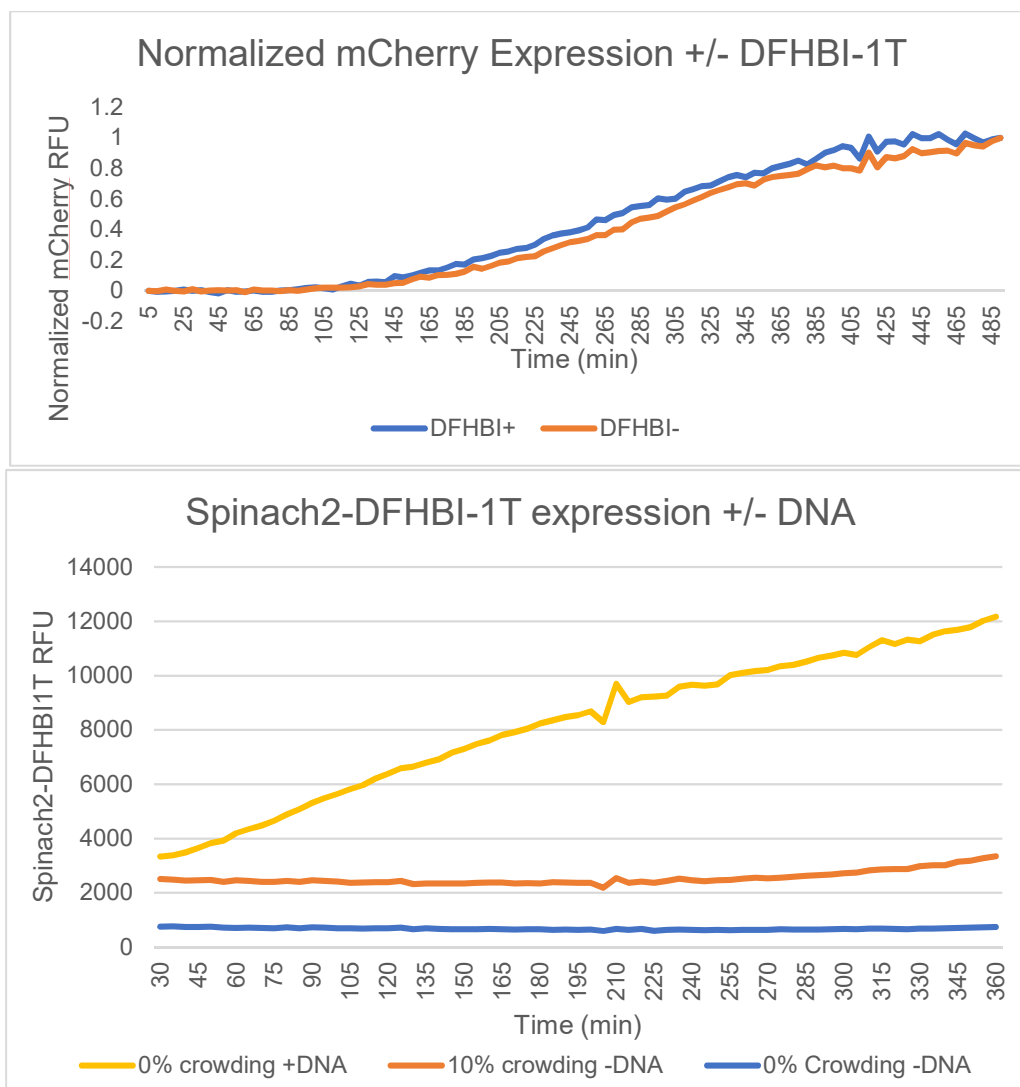


Figure S6: Control Experiments for Cell-free reactions. Top) Normalized expression of mCherry in the Promega S30 T7 High-Yield Protein Expression System. Traces are averages of triplicate reactions. The presence of DFHBI-1T did not significantly affect the shape of the average protein traces, indicating that the presence of the fluorophore does not have a significant effect on the translational timescale. Bottom) Spinach2-DFHBI-1T fluorescence in cell-free reactions in presence and absence of DNA. All reactions initially have some autofluorescence which appears to photobleach to a uniform background level after the first few time points. The presence of Ficoll-70 increases this baseline level of fluorescence, but cell-free experiments in the absence of plasmid do not increase significantly in fluorescence over time. This indicates that autofluorescence from Ficoll-70 does not substantially affect the zeroed data.

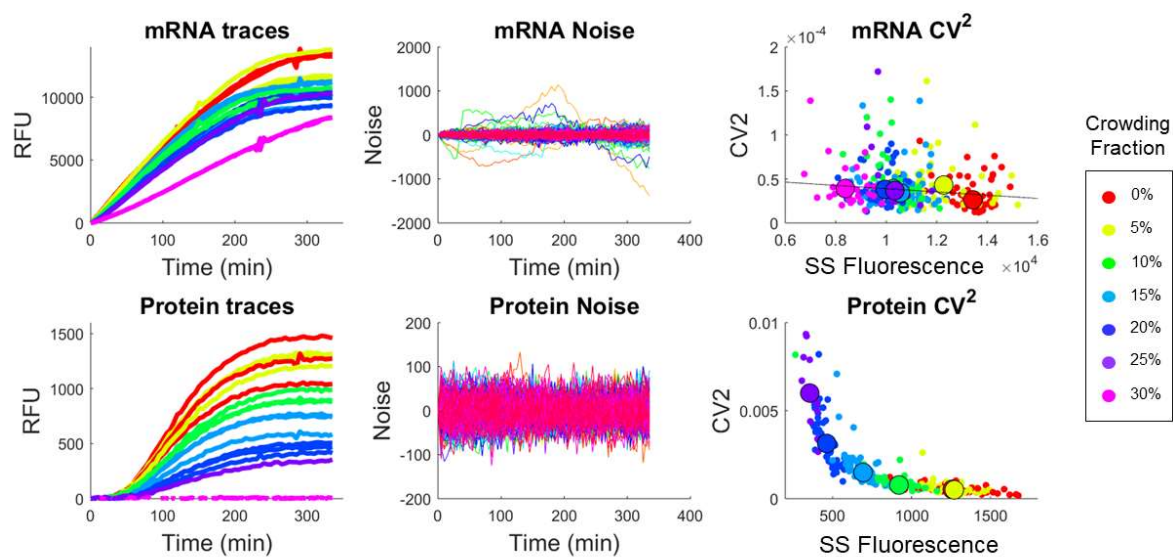


Figure S7: mRNA and Protein Expression in PURE System. A single experiment consisted of 16 traces from 15uL microplate well reactions. Fluorescent reads were performed at 495nm and 630nm. The method for performing noise analysis has been detailed in previous work^{8, 13, 15-17}. The first panel shows the average timescale trace for each 16-reaction experiment, colored by crowding fraction. The average trace is corrected for the transient and subtracted from each individual reaction trace to create noise traces (shown as individually colored traces in the second panel). These individual traces are plotted as individual points in “noise space”, or CV^2 vs steady-state fluorescence, colored by crowding fraction. Large dots represent the average for each crowding fraction group.

EXPERIMENTAL METHODS SUPPLEMENT

Gene Structure

The pRSETb-mCherry-Spinach2 plasmid was constructed using an in-house pRSET-b backbone with an mCherry insertion. The restriction enzymes EcoRI and HindIII were used to insert the Spinach2 oligomer sequence, which was constructed by IDT DNA. The publicly available sequence for this aptamer and framing tRNA scaffolds was taken from the Jaffery Lab website¹⁸. The aptamer sequence was inserted downstream of the protein sequence to ensure that a full transcript of the mCherry sequence was produced.

Gene Sequence (From T7 Promoter to T7 terminator)

```
TAATACGACTCACTATAGGGAGACCACAACGGTTTCCCTCTAGAATAATTTGTTTAACTTTAAGAAGGAGATATACATATGCG
GGGTTTCTCATCATCATCATCATCATGGTATGGCTAGCATGACTGGTGGACAGCAAATGGGTGCGGATCTGTACGACGATGACG
ATAAGGATCCCAGCCACCATGGTGAACAAGGGCGAGGAGGATAACATGGCCATCATCAAGGAGTTCATGCGCTTCAAGGTGCAC
ATGGAGGGCTCCGTGAACGGCCACGAGTTCGAGATCGAGGGCGAGGGCGAGGGCCGCCCCCTACGAGGGCACCCAGACCCG
CAAGCTGAAGGTGACCAAGGGTGGCCCCCTGCCCTTCGCTGGGACATCCTGTCCCCTCAGTTCATGTACGGCTCCAAGGCCT
ACGTGAAGCACCCCGCCGACATCCCCGACTACTTGAAGCTGTCCTTCCCCGAGGGCTTCAAGTGGGAGCGCGTGATGAACTTC
GAGGACGGCGGCGTGGTGACCGTGACCCAGGACTCCTCCTGCAGGACGGCGAGTTCATCTACAAGGTGAAGCTGCGCGGC
ACCAACTTCCCCTCCGACGGCCCCGTAATGCAGAAGAAGACCATGGGCTGGGAGGCCTCCTCCGAGCGGATGTACCCCGAGG
ACGGCGCCCTGAAGGGCGAGATCAAGCAGAGGCTGAAGCTGAAGGACGGCGGCCACTACGACGCTGAGGTCAAGACCACCT
ACAAGGCCAAGAAGCCCGTGCAGCTGCCCGGCGCCTACAACGTCAACATCAAGTTGGACATCACCTCCCACAACGAGGACTAC
ACCATCGTGGAACAGTACGAACGCGCCGAGGGCCGCACTCCACCGGCGGCATGGACGAGCTGTACAAGTAAGAATTGAGC
TCGAGATCTGCAGCTGGTACCATGGCCCCGATAGCTCAGTCGGTAGAGCAGCGGCCGGATGTAAGTGAATGAAATGGTGAAG
GACGGGTCCAGTAGGCTGCTTCGGCAGCCTACTTGTGAGTAGAGTGTGAGCTCCGTAAGTACTAGTACATCCGGCCGCGGGTCC
AGGGTTCAAGTCCCTGTTCCGGGCGCCAAAGCTTGATCCGGCTGCTAACAAAGCCCGAAAGGAAGCTGAGTTGGCTGCTGCCA
CCGCTGAGCAATAACTAGCATAACCCCTTGGGGCCTTAAACGGGTCTTGAGGGGTTTTTTG
```

Gene Preparation

A plasmid midiprep kit (Quantum Prep Plasmid Midiprep Kit, BioRad) was used to isolate pRSETb-mCherry-Spinach2 from Top 10 *E. coli* following manufacturer's instructions. The plasmid was purified by Isopropanol precipitation and the pellet washed with 70% Ethanol. The plasmid was resuspended in nuclease free water at a concentration of 1000 ng/ μ L.

CFPS Experiment Formulation

Cell-free experiments used the PURExpress cell-free protein expression kit (NEB) diluted with nuclease-free water to the maximum manufacturer-suggested reaction volume of 30 μ L per reaction. A final plasmid concentration of 8.33 ng/ μ L was used for all reactions (250ng plasmid/reaction). DFHBI-1T (Lucerna, Inc) was diluted in DMSO and used in the reaction at a final concentration of ~13 μ M. From these ratios,

experiments were scaled up to a total volume of 300 μ L. For each experiment, a 300 μ L master mix was created and divided into 15 μ L microplate well reactions.

The assembled reactions were applied to a 384-well microplate (Corning #3540, black, clear-bottom) in 15 μ L aliquots. A 12-hour kinetic read was performed in a microplate reader (Perkin-Elmer EnSpire Multimode Plate Reader), with fluorometric reads at 495nm and 630nm every 5 minutes. Reactions were incubated at 30°C with 2 minutes shaking. The microplate was covered with a qPCR film to prevent evaporation.

Cell-Free Protein Synthesis (CFPS) previous work and control experiments

Similar gene structures to the one constructed for this paper have been examined in cell-free conditions^{19, 20}. Of particular relevance was Van Nies et al. 2013 which used a yellow fluorescent protein and an earlier version of the Spinach aptamer and DFHBI. The final concentration of DFHBI-1T used in this work (13 μ M) approximates the DFHBI concentration used in the previous work (20 μ M).

The CFPS experiments were initially tested for the effects of Spinach2-DFHBI-1T activity in the Promega S30 T7 High-Yield Protein Expression System. In order to determine how protein expression timescales were affected by the presence or absence of DFHBI-1T, reactions were run with and without the fluorophore, finding that difference in normalized timescales for both conditions are not significant (Fig. S6, top). In the PURExpress system, reactions were performed in the presence and absence of DNA and crowders in order to determine background fluorescence levels in the Spinach2-DFHBI-1T range (Fig. S6, bottom).

Vesicle Preparation Methods

Vesicle preparation was adapted from Nishimura et al. 2012²¹; the experiment was modified to observe mRNA and protein expression simultaneously. Briefly, vesicles are prepared by preparing the PURE System as described previously (“Inner solution”), with the addition of sucrose in order to aid visualization of vesicles in brightfield images. The inner solution is placed into a paraffin oil mixture containing phospholipids (POPC, Avanti Polar Lipids) and then vortexed to create a disperse population of vesicles. This “oil phase” vesicle emulsion is layered onto an aqueous “Outer Solution” mixture

balanced with the aqueous Inner solution. The layered solutions are then centrifuged for 20 minutes at high speed (~14k g) at 4C. Vesicles are collected by pipetting from the bottom layer. The majority of vesicle diameters range from approximately 5-30 μm .

TABLE S2: Vesicle Reactants

Inner Solution	Outer Solution
10 μL PURE Solution A, 7.5 μL PURE Solution B, 250 ng pRSETb-mCherry-Spinach2 plasmid 0.5 μL DFHBI-1T (1.56 mM) 5 μL Sucrose (1 M), and filled to 30 μL with Nuclease-free water.	3.6 mL Amino Acid mix (50 mM), 4.9 mL ATP (460 mM), 3.0 mL GTP (500 mM), 1.5 mL CTP (500 mM), 1.5 mL UTP (500 mM), 3.6 mL Spermidine (250 mM), 7.5 mL Creatine Phosphate (1 M), 9 mL DTT (100 mM), 1.5 mL Folinic Acid (4 mg/mL), 168 mL Potassium Glutamate (1 M), 22.6 mL Magnesium Acetate (0.5 M), 60 mL HEPES (1 M), 120 mL Glucose (1 M), and filled to 600 mL with nuclease-free water.

Vesicles were imaged in a method similar to that described in Caveney et al., 2016¹⁵. Vesicles in the outer solution mixture were pipetted onto a glass coverslip. The droplet containing the vesicles was surrounded by a ~2mm PDMS spacer, and another coverslip was applied on top of the spacer to create an airtight chamber. This setup prevents evaporation and global drift in the imaged vesicle solution. ImageJ was used to perform the analytical steps of the intensity image taken from fluorescence values of the mRNA and Protein. For the Fig. 4 analytical images of mRNA in vesicles, a square 1444 pixel region of interest was selected in the interior of two representative vesicles, one in an uncrowded (0%) reaction and the other in a mildly crowded 5% reaction. The intensity values of the ROIs were extracted and analyzed in MATLAB. 3D representations of the vesicles may be constructed from z-stack imaging, simplifying the estimation of vesicle diameter. The vesicles rest on the glass coverslip; they are largely spherical. Larger vesicles ($d > 20$ microns) tend to be easier to image because they settle on the glass quickly and do not move significantly for several hours.

References

- [1] Thattai, M., and Van Oudenaarden, A. (2001) Intrinsic noise in gene regulatory networks, *Proceedings of the National Academy of Sciences* 98, 8614-8619.
- [2] Singh, A., Razoooky, B., Cox, C. D., Simpson, M. L., and Weinberger, L. S. (2010) Transcriptional bursting from the HIV-1 promoter is a significant source of stochastic noise in HIV-1 gene expression, *Biophysical journal* 98, L32-L34.
- [3] Ozbudak, E. M., Thattai, M., Kurtser, I., Grossman, A. D., and van Oudenaarden, A. (2002) Regulation of noise in the expression of a single gene, *Nat. Genet.* 31, 69.
- [4] Hasty, J., and Collins, J. J. (2002) Translating the noise, *nature genetics* 31, 13.
- [5] So, L., Ghosh, A., Zong, C., Sepúlveda, L. A., Segev, R., and Golding, I. (2011) General properties of transcriptional time series in *Escherichia coli*, *Nat. Genet.* 43, 554.
- [6] Taniguchi, Y., Choi, P. J., Li, G. W., Chen, H., Babu, M., Hearn, J., Emili, A., and Xie, X. S. (2010) Quantifying *E. coli* proteome and transcriptome with single-molecule sensitivity in single cells, *Science* 329, 533.
- [7] Dar, R. D., Razoooky, B. S., Weinberger, L. S., Cox, C. D., and Simpson, M. L. (2015) The Low Noise Limit in Gene Expression, *PLoS One* 10, e0140969.
- [8] Dar, R. D., Razoooky, B. S., Singh, A., Trimeloni, T. V., McCollum, J. M., Cox, C. D., Simpson, M. L., and Weinberger, L. S. (2012) Transcriptional burst frequency and burst size are equally modulated across the human genome, *Proc. Natl. Acad. Sci. U. S. A.* 109, 17454.
- [9] Dar, R. D., Shaffer, S. M., Singh, A., Razoooky, B. S., Simpson, M. L., Raj, A., and Weinberger, L. S. (2016) Transcriptional bursting explains the noise-versus-mean relationship in mRNA and protein levels, *PloS one* 11, e0158298.
- [10] Hansen, M. M., Meijer, L. H., Spruijt, E., Maas, R. J., Rosquelles, M. V., Groen, J., Heus, H. A., and Huck, W. T. (2016) Macromolecular crowding creates heterogeneous environments of gene expression in picolitre droplets, *Nature nanotechnology* 11, 191-197.
- [11] Simpson, M. L., Cox, C. D., and Sayler, G. S. (2003) Frequency domain analysis of noise in autoregulated gene circuits, *Proceedings of the National Academy of Sciences* 100, 4551-4556.
- [12] Dauty, E., and Verkman, A. (2004) Molecular crowding reduces to a similar extent the diffusion of small solutes and macromolecules: measurement by fluorescence correlation spectroscopy, *Journal of molecular recognition* 17, 441-447.
- [13] Karig, D. K., Iyer, S., Simpson, M. L., and Doktycz, M. J. (2012) Expression optimization and synthetic gene networks in cell-free systems, *Nucleic acids research* 40, 3763-3774.
- [14] Sun, Z. Z., Hayes, C. A., Shin, J., Caschera, F., Murray, R. M., and Noireaux, V. (2013) Protocols for implementing an *Escherichia coli* based TX-TL cell-free expression system for synthetic biology, *J. Visualized Exp.*, e50762.
- [15] Caveney, P. M., Norred, S. E., Chin, C. W., Boreyko, J. B., Razoooky, B. S., Retterer, S. T., Collier, C. P., and Simpson, M. L. (2016) Resource Sharing Controls Gene Expression Bursting, *Acs Synth Biol.*
- [16] Norred, S. E., Caveney, P. M., Retterer, S. T., Boreyko, J. B., Fowlkes, J. D., Collier, C. P., and Simpson, M. L. (2015) Sealable Femtoliter Chamber Arrays for Cell-free Biology, *J. Visualized Exp.*, e52616.
- [17] Weinberger, L. S., Dar, R. D., and Simpson, M. L. (2008) Transient-mediated fate determination in a transcriptional circuit of HIV, *Nat. Genet.* 40, 466.
- [18] Strack, R. L., Disney, M. D., and Jaffrey, S. R. (2013) A superfolder Spinach2 reveals the dynamic nature of trinucleotide repeat-containing RNA, *Nature methods* 10, 1219-1224.
- [19] van Nies, P., Nourian, Z., Kok, M., van Wijk, R., Moeskops, J., Westerlaken, I., Poolman, J. M., Eelkema, R., van Esch, J. H., and Kuruma, Y. (2013) Unbiased Tracking of the

Progression of mRNA and Protein Synthesis in Bulk and in Liposome-Confined Reactions, *ChemBioChem* 14, 1963-1966.

[20] Chizzolini, F., Forlin, M., and Mansy, S. S. (2016) Cell-free translation is more variable than transcription, *bioRxiv*.

[21] Nishimura, K., Tsuru, S., Suzuki, H., and Yomo, T. (2014) Stochasticity in gene expression in a cell-sized compartment, *Acs Synth Biol* 4, 566-576.